

- IDEALFUEL -

Lignin as a feedstock for renewable marine fuels

GRANT AGREEMENT No. 883753

HORIZON 2020 PROGRAMME - TOPIC LC-SC3-RES-23-2019

“Development of next generation biofuel and alternative renewable fuel technologies for aviation and shipping”



Deliverable Report

D2.5 – Scientific publication compiled from data from
D2.1-2.4



This project has received funding from the European Union's Horizon 2020 research and innovation programme under grant agreement No 883753

Deliverable No.	IDEALFUEL D2.5	
Related WP	WP2	
Deliverable Title	Scientific publication compiled from data from D2.1-2.4	
Deliverable Date	15-04-2024	
Deliverable Type	REPORT	
Dissemination level	Public (PU)	
Written By	Alexandra Radu (TUE)	02/04/2024
Checked by	Michael Boot (TUE)	03/04/2024
Reviewed by	Panos Kouris (VER)	05/04/2024
Approved by	Roy Hermanns (TUE)	25/04/2024
Status	Final	25/04/2024

Disclaimer/ Acknowledgment



Copyright ©, all rights reserved. This document or any part thereof may not be made public or disclosed, copied or otherwise reproduced or used in any form or by any means, without prior permission in writing from the IDEALFUEL Consortium. Neither the IDEALFUEL Consortium nor any of its members, their officers, employees or agents shall be liable or responsible, in negligence or otherwise, for any loss, damage or expense whatever sustained by any person as a result of the use, in any manner or form, of any knowledge, information or data contained in this document, or due to any inaccuracy, omission or error therein contained.

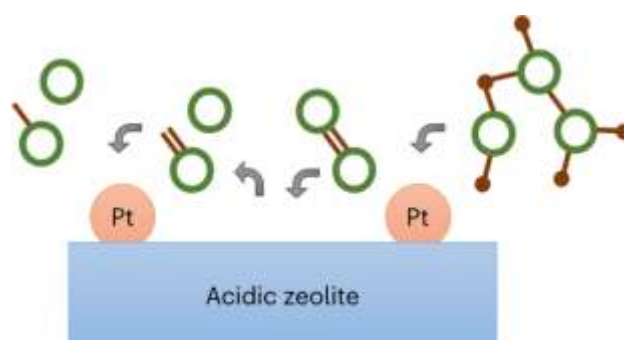
All Intellectual Property Rights, know-how and information provided by and/or arising from this document, such as designs, documentation, as well as preparatory material in that regard, is and shall remain the exclusive property of the IDEALFUEL Consortium and any of its members or its licensors. Nothing contained in this document shall give, or shall be construed as giving, any right, title, ownership, interest, license or any other right in or to any IP, know-how and information.

This project has received funding from the European Union's Horizon 2020 research and innovation programme under grant agreement No 883753. The information and views set out in this publication does not necessarily reflect the official opinion of the European Commission. Neither the European Union institutions and bodies nor any person acting on their behalf, may be held responsible for the use which may be made of the information contained therein.

Publishable summary

The EU H2020 project IDEALFUEL aims to develop an efficient and low-cost chemical pathway to convert lignocellulosic biomass into a Biogenic Heavy Fuel Oil (Bio-HFO) - with ultra-low sulfur levels - that can be used as drop-in fuel in the existing maritime fleet. While technical lignins are cheap and available in large quantities, their characteristics are not suitable for the development of high-performance marine fuels. Among others, these lignins suffer from low solubilities, large molecular weight, high sulfur content and are generally non-uniform in their chemical nature. One strategy consists in solvent fractionation of technical lignins and/or woody biomass to extract a high-quality fraction, which can be more suitable for fuels applications. A second strategy consists in the production of high-quality lignin from biomass with alternative bio-refining process. Within IDEALFUEL, the partners selected lignin/biomass solvolysis and Aldehyde-Assisted Fractionation (AAF) as the most relevant technologies for the production of high-performance lignin for fuel applications. Technical lignin solvolysis to an intermediate crude lignin oil (CLO) prior to the bio-HFO production, is one of the process solutions within IDEALFUEL project coordinated by WP2. The AAF process enables the production of an uncondensed lignin polymer stream from lignocellulosic biomass. In a second steps, a selective catalytic depolymerization process produces a well-defined stream of lignin oligomers. These AAF oligomers via the CLO process, can be used as feedstock for bio-HFO production for the maritime industry.

In this report, the scientific content of which having been published in *Nature Chemical Engineering*¹, we examine the cracking of the carbon-carbon bonds in the AAF oligomers. Carbon-carbon bonds, ubiquitous in lignin, limit monomer yields from current depolymerization strategies, which mainly target C-O bonds. Selective cleavage of the inherently inert σ -type C-C bonds without pre-functionalization remains challenging. Here we report the breaking of C-C bonds in lignin obtained upon initial disruption of labile C-O bonds, achieving monocyclic hydrocarbon yields up to an order of magnitude higher than previously reported.



The use of a Pt (de)hydrogenation function leads to olefinic groups close to recalcitrant C-C bonds, which can undergo β -scission over zeolitic Brønsted acid sites. After confirming that this approach can selectively cleave common C-C linkages ($5-5'$, $\beta-1'$, $\beta-5'$ and $\beta-\beta'$) in lignin skeletons, we demonstrate its utility in the valorization of various representative lignins. A techno-economic analysis shows the promise of our method for producing gasoline- and jet-range cycloalkanes and aromatics, while a life-cycle assessment confirms its potential for CO₂-neutral fuel production.

¹ Luo, Z., Liu, C., Radu, A. *et al.* Carbon-carbon bond cleavage for a lignin refinery. *Nat Chem Eng* **1**, 61–72 (2024).

<https://doi.org/10.1038/s44286-023-00006-0>

Contents

1	Introduction.....	5
2	Methods and Results.....	7
3	Conclusions.....	19
	Acknowledgement.....	20

Table of Figures

Figure 1 - Valorization of lignocellulosic biomass.....	6
Figure 2 - Reductive C–C cleavage of 2,2'-biphenol (1).....	10
Figure 3 - DFT study of the reaction mechanism of C–C bond cleavage.....	11
Figure 4 - Substrate scope for reductive C–C cleavage.....	13
Figure 5 - Reductive cleavage of AAF oligomers.....	15
Figure 6 - Process layout and details of the proposed AAF oligomers refinery.	17

1 Introduction

Lignocellulosic biomass, the most abundant renewable feedstock on Earth, can replace fossil resources to produce fuels, chemicals and materials. It consists of cellulose (35%–50%), hemicellulose (20%–35%) and lignin (10%–25%). Traditionally, lignin is burned to generate power, mainly in the pulp and paper industry, where the cellulose part of biomass is the main product. The advent of second-generation biorefineries will generate more lignin waste, which needs to be converted to valuable products to render these operations economically viable. Depolymerization of lignin into fragments with lower molecular mass suitable for downstream processing is one of the most promising approaches to obtaining value-added products from lignin side streams. Lignin is randomly linked by C–C bonds (β -5', β -5', β -1' and β - β ') and C–O bonds (β -O-4', α -O-4' and 4-O-5') with respective contents of 20–40% and 60–80% in lignocellulosic biomass. Cleaving the relatively labile β -O-4' bonds is the primary depolymerization strategy for obtaining monomers. The 'maximum monomer' yield based on cleaving these bonds can be approximated as the square of the fraction of β -O-4' bonds. For lignin with a relatively high β -O-4' content of 70%, the maximum monomer yield will be 49%. Extracting uncondensed lignin with a high β -O-4' content during biomass fractionation can facilitate the subsequent production of lignin monomers. Biomass fractionation in paper and pulp manufacture ('harsh' fractionation) involves using mineral acids or bases at relatively high temperatures to remove lignin and hemicellulose from the lignocellulosic matrix. Under such severe conditions, lignin undergoes irreversible condensation, where the C–O bonds break and new recalcitrant C–C bonds form, yielding a highly condensed lignin. Mild fractionation, including ammonia-based fractionation, ionic liquid-assisted fractionation, γ -valerolactone assisted hydrolysis and organosolv approaches, results in more reactive (that is, less condensed) lignins, in which the disruption of C–O bonds and the concurrent formation of reactive intermediates is diminished. The drawback of mild fractionation is that the yield of isolated lignin with a relatively high β -O-4' content is usually low. Increasing the extent of delignification requires harsher conditions, which reduces the β -O-4' content in the extracted lignin. This trade-off was demonstrated in a recent study covering types of lignin, where conservation of high β -O-4' content was accompanied by a low yield of isolated lignin. The lignin-first strategy, which has emerged recently, focuses on separating lignin from the lignocellulosic matrix, resulting in a lignin oil and a solid carbohydrate pulp. A promising lignin-first approach comprises reductive catalytic fractionation (RCF), where lignin-carbohydrate bonds are broken by hydrogenolysis. At the same time, the released lignin fragments are further hydrogenated to a lignin oil with a yield close to the maximum monomer yield based on the β -O-4' content. However, this lignin-first strategy is also hampered by the inability to cleave C–C bonds, which leaves a highly condensed, high-molecular-weight technical lignin residue with many C–C linkages. The C–C bonds in technical lignin can be categorized into aryl-aryl (β -5'), aryl-alkyl (β -5') and alkyl-alkyl (β -1' and β - β '). Their high dissociation energies in the 226–494 kJ mol⁻¹ range hamper the optimal valorization of this important renewable resource. To extract more monomers from technical lignin, approaches that can cleave the recalcitrant C–C bonds are needed. Samec and colleagues reported the oxidative cleavage of aryl-alkyl and alkyl-alkyl linkages in lignin with the formation of 2,6-dimethoxybenzoquinone in a yield of 18%, corresponding to a total monomer yield of 132% relative to the maximum monomer yield. However, the oxidation approach only cleaved C–C bonds in lignin fragments containing free phenolic groups but not aryl-aryl bonds. Another drawback is that the stoichiometric oxidant must be regenerated. It would be highly desirable if the scission of various C–C bonds could be achieved by one-pot reductive chemistry. The main challenge is to break these C–C bonds selectively. Typically, the high reaction temperatures (>310 °C) required to break C–C bonds lead to extensive cracking and low yields of desirable ring products. Compared to cracking, catalytic hydrogenolysis at milder conditions (\leq 310 °C) can be carried out with higher selectivity. Dong and colleagues used a rhodium-based catalyst to break the aryl-aryl bond in 2,2'-biphenols, which are abundant in lignin, and unstrained aryl-alkyl bonds in phenolic resins. However, this method cannot break alkyl-alkyl bonds.

Concerns for the practical implementation of this innovative approach are that the catalyst requires the absence of water and the use of substantial amounts of phosphinites as a modifying group. Under relatively mild reaction conditions of 310 °C and 5 bar H₂, a Ru/NbOPO₄ catalyst was reported to cleave C–C bonds in lignin selectively, resulting in the formation of monocyclic hydrocarbons in a yield of 8.0–9.9% (Fig. 1b). The total monomer yield achieved was 124–153% relative to the maximum monomer yield. Despite the high selectivity for cleaving aryl–aryl and aryl–alkyl bonds, the catalyst displayed no activity for breaking alkyl–alkyl bonds, which limits the monomer yield. Thus, there remains a need for a hydrogenation approach to selectively disrupt all three types of C–C linkage in lignin under mild reaction conditions. In this Article we report a mild and reductive catalytic approach employing a bifunctional Pt/H-MOR catalyst to depolymerize technical lignin to obtain monomers in a 2–11-times higher yield than reported in the literature. The utility of this approach is illustrated by selective cleavage of aryl–aryl, aryl–alkyl and alkyl–alkyl in seven different lignins at a relatively low temperature of 300 °C. Mechanistic studies show that the Brønsted acid sites in H-MOR can directly cleave aryl–alkyl bonds. Pt/H-MOR catalyzes the cleavage of aryl–aryl and alkyl–alkyl compounds via bifunctional catalysis, where Pt hydrogenates aryl moieties and introduces double bonds in alkyl ones, followed by acid-catalyzed β-scission. This approach substantially improves the monomer yield, with the best results constituting a 58–409% increase over the conventional maximum monomer yield obtainable for the investigated lignins.

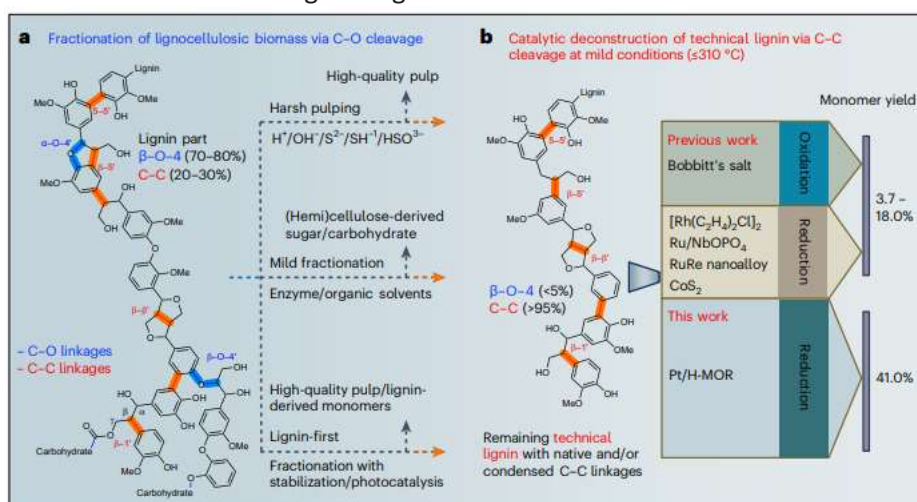


Figure 1 - Valorization of lignocellulosic biomass

a, State-of-the-art approaches for the fractionation of lignocellulosic biomass via C–O cleavage. The C–C and C–O bonds in lignin are highlighted in red and blue, respectively. b, Current and proposed catalytic approaches for the deconstruction of technical lignin via C–C cleavage under mild conditions (≤310 °C).

2 Methods and Results

Preparation of catalysts

Pt was loaded on various support materials by wetness impregnation. In a typical synthesis, 1.0 g of H-MOR was suspended in a tetraammineplatinum(II) nitrate solution, prepared by dissolving 0.0198 g ($\text{Pt}(\text{NH}_3)_4(\text{NO}_3)_2$) in 20 ml of deionized water. After stirring for 2 h, the mixture was dried at 80 °C overnight. The powder was calcined in flowing artificial air at 300 °C for 4 h, followed by reduction in a 50 vol% H_2 in He flow at 300 °C for 4 h (1 °C min^{-1}). The Pt content of Pt/H-MOR was ~ 1 wt%. Na-exchanged H-MOR catalyst was prepared by three times ion exchange with a 1 M NaNO_3 solution at 40 °C for 24 h, followed by centrifugation and drying at 80 °C overnight. The Pt/Na-MOR zeolite was obtained in the same way as Pt/H-MOR. Pt was loaded on other support materials in the same way. Ru/H-MOR, Ni/H-MOR and Cu/H-MOR were obtained by incipient wetness impregnation using aqueous solutions of RuCl_3 , $\text{Ni}(\text{NO}_3)_2 \cdot 6\text{H}_2\text{O}$ and $\text{Cu}_2(\text{NO}_3)_4 \cdot 5\text{H}_2\text{O}$, respectively, of appropriate concentration under vigorous stirring for 2 h. The resulting solid mixture was dried, calcined and reduced in the same way as the Pt-containing zeolites, except for the Ru/H-MOR zeolite, which was calcined in He.

Conversion of lignin model compounds and lignins

In lignin model compound conversion studies, the substrate (20 mmol l^{-1}) and catalyst (50 mg) were loaded into a 100-ml Parr reactor with n-pentane (40 ml) as the solvent. Once closed, the reactor was purged with N_2 five times and charged with H_2 at 40 bar. The reactor was heated to the desired temperature, followed by a dwell under stirring (650 r.p.m.). Liquid products for gas chromatography (GC) analysis were sampled during the experiment. After the reaction, the reactor was cooled in an ice bath until the temperature was below 10 °C, at which time the gaseous products were collected for GC analysis. In lignin conversion studies, 1.0 g of lignin powder was mixed with 500 mg of solid catalyst. The remaining procedure was the same as described above.

^1H - ^{13}C HSQC NMR of lignin

Approximately 100 mg of dried lignin was dissolved in 0.7 ml of dimethylsulfoxide- d_6 (DMSO- d_6). NMR spectra were recorded using a VARIAN INOVA 500-MHz spectrometer equipped with a 5-mm ID Auto ID PFG probe (128 scans acquired from 0 to 16 ppm in the F2 (^1H) dimension with 1,200 data points (acquisition time 10 ms) and 44 scans with 0 to 200 ppm in the F1 (^{13}C) dimension with 256 t_1 increments (acquisition time 10 ms) and 2-s relaxation time). Data were processed using MestreNova software. The DMSO solvent peak was used as an internal reference ($\delta\text{C} = 39.5$ ppm, $\delta\text{H} = 2.50$ ppm). Semi-quantitative analysis of the HSQC NMR spectra was done by integration of the correlation peaks in the different regions of the spectra according to literature methods. The relative quantity of side chains involved in the inter-unit and terminal substructures is expressed as a number per 100 aromatic units (S + G).

Derivatization and analysis of dimers in lignin oils

Derivatization was performed as described previously. Dried lignin oil samples were prepared for dissolving in dichloromethane to obtain a 10-mg-ml $^{-1}$ solution. Six hundred microliters of 10-mg-ml $^{-1}$ lignin oil solution were added to a 2-ml GC vial, followed by the addition of 50 μl of pyridine and 100 μl of silylating agent. N,O-bis(trimethylsilyl) trifluoroacetamide (BSTFA) with 1% trimethylchlorosilane was used as the silylating agent. As this compound reacts readily with water, BSTFA was applied immediately after opening the cap, followed by immediately closing the GC vial. The lignin oil, pyridine and BSTFA solution were then heated for 30 min at 50 °C before being injected on the GC-MS.

Computational methods

Periodic DFT calculations were performed using the Vienna Ab initio Simulation Package (VASP, version 5.4.4). The Perdew–Burke–Ernzerhof (PBE) functional was combined with the projector augmented wave (PAW) method. The cutoff energy of the plane-wave basis set was set to 500 eV. The Brillouin zone sampling was restricted to the Γ point. Van der Waals interactions were described by the DFT-D3 (BJ) method. Structures were assumed to be converged when the force on each atom was below 0.05 eV \AA^{-1} . The minimum-energy reaction paths and corresponding transition states were determined by the climbing image nudged elastic band (CI-NEB) method. The maximum energy geometries along the reaction path from CI-NEB calculations were further optimized using a quasi-Newton algorithm. FAU zeolite was simulated using a rhombohedral 48 T unit cell (Si48O96). Brønsted acid sites were introduced by replacing one of the lattice Si with an Al atom with a charge-compensating proton (H^+) being added to the anionic oxygen site (Supplementary Fig. 9). The cell parameters were first optimized, followed by complete geometry optimization with guest molecules with fixed lattice parameters ($a = b = c = 17.29 \text{ \AA}$, $\alpha = \beta = \gamma = 60^\circ$).

Process design details for TEA and LCA

The process simulations were performed using Aspen Plus (V10.0). ENVIRON was used as a method filter, and METCBAR was chosen as the global unit. For modeling the equilibrium data of jet fuel and gasoline, the Soave–Redlich–Kwong equation of state (SRK) method is used. Details on the assumptions for these process simulations and input data are described in the Supplementary Information. Briefly, the reactors were operated in a steady state, assuming uniform temperatures and pressures in the reactors. The units were designed to process 2,000 tons of lignin per day. The reaction conditions for the hydrotreatment step were 300 °C, 4 MPa and a reaction time of 24 h. The lignin/n-pentane/hydrogen mass ratio was 1/25.2/0.19. The stripping conditions used for gas–liquid separations were 25 °C and 3 bar. The stripping conditions for the liquid–liquid separation was 40 °C and a vapor fraction of 0.9. The jet fuel and gasoline/water mass ratio during separation is 1/0.095. The combustion of C_1 – C_4 gas, H_2 and lignin residues was carried out at 900 °C and 1 bar. In the system, excess heat is used to produce steam as a by-product. Moreover, gaseous products (C_1 – C_4 gas and a small amount of hydrogen) and lignin residues are fed into the combustion chamber to supply heat.

Methodology for TEA

TEA includes a detailed process flow diagram (based on research data), rigorous materials and energy balance calculations (via Aspen Plus simulation tools), capital and project cost estimation (percentages of the total equipment costs and revenues), and calculations of a net present value of zero (NPV) and a minimum fuel selling price. The project length is 20 years. The operation time is 7,884 h per year. The total plant cost includes equipment cost, other direct costs (installation, building and auxiliaries) and indirect costs (engineering and contingency). Direct costs are specified as 50% of equipment cost. Indirect costs are calculated to be 30% of equipment cost and direct costs. The monetary price of the products and raw materials is considered as the average market price in 2020. The lifetime of the Pt/H-MOR catalyst was assumed to be one year.

Methodology for LCA

The system boundaries encompass a cradle-to-gate approach (Supplementary Fig. 29), meaning that the analysis considers all stages in the life cycle of the products. These stages include hydrogenolysis of the isolated lignin obtained during fractionation of hardwood using isobutyraldehyde protection, transportation of AAF1 oligomers, and the production of jet fuel and gasoline. The first two processes do not consider CO_2 emissions, because AAF1 oligomers are considered a by-product. The production of jet fuel and gasoline (Supplementary Fig. 24 and Fig. 6a) includes hydrotreatment, liquid–solid separation, liquid–liquid fractionation, hydrogen pressure swing adsorption (PSA), liquid and gas circulation, and combustion.

The input is composed of catalyst, hydrogen, pentane and electricity. The CO₂ emissions for the usage of jet fuel and gasoline are not included due to the carbon-neutral property of AAF1 oligomers. The GWP was studied using SimaPro software (9.4.0.1). The Ecoinvent 3 and Industry data 2.0 LCI databases were used to determine the environmental impact of the existing technologies and production processes. 'Cut-off, S' is selected as the model to analyze the GWP of the feedstock. The data in the process are determined from laboratory experiments, which are simulated on an industrial scale accompanied by the TEA. The allocation of CO₂ emission is based on the economic value of the products. The assessment method used was IPCC 2013 GWP.

Results and discussion

For catalyst screening, we used a model lignin dimer (2,2'-biphenol, 1), representative of the 5–5'-linked units (C–C bonds) ubiquitous in lignin and with the highest bond dissociation energy in the 481–494 kJ mol⁻¹ range. The reductive cleavage of C–C bonds in 1 was evaluated at a temperature of 260 °C and an H₂ pressure of 40 bar using n-pentane as the solvent. Figure 2a shows the results for the different catalysts explored. The most important physicochemical properties of these catalysts are reported in Extended Data Table 1 and Supplementary Fig. 1. Without a catalyst, 1 was not converted under these conditions. In the presence of Pt/SiO₂, 1 was completely converted to mainly bicyclohexyl (10) and a small amount of cyclopentylmethylcyclohexane (11). With H-MOR as the catalyst, 1 was quantitatively dehydrated to dibenzofuran (7). By combining Pt/SiO₂ and H-MOR, monomers such as cyclohexane (13) and methylcyclopentane (14) were obtained with a total yield of 8.0%. The monomer yield from the conversion of 1 improved to 86.3% when Pt/H-MOR was used instead of a physical mixture of Pt/SiO₂ and H-MOR. Its non-acidic counterpart, Pt/Na-MOR, did not afford monomers. The low activity obtained with Pt/SiO₂–Al₂O₃ can be attributed to the low acidity of amorphous silica–alumina. Other common Pt/acid–base catalysts, such as Pt/Nb₂O₅ and Pt/TiO₂, did not result in monomers either. The preference for Pt/H-MOR was further compared by varying the Brønsted acid support and the metal (Supplementary Note 1). It was verified that the n-pentane solvent was not converted to monomers by carrying out the experiment without 1 with Pt/H-MOR (Supplementary Figs. 2 and 3 and Supplementary Table 2). A recent study reported a Pt/CDC–SiC (carbide-derived carbon–SiC composite) catalyst that achieved a monomer yield of 49.3 wt% by cleaving the C–C bond in 1 assisted by microwave irradiation.

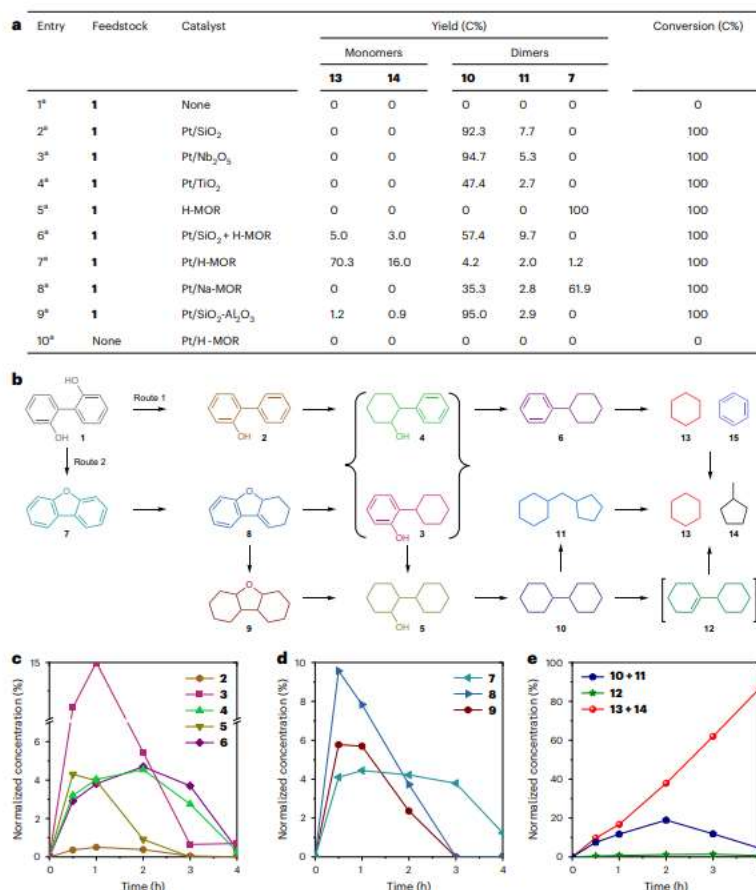


Figure 2 - Reductive C–C cleavage of 2,2'-biphenol (1)

a, Reductive cleavage of 1 using various catalysts. Conversion and yield are defined in Supplementary Section 1.3. b, Proposed reaction pathways for the conversion of 1 over Pt/H-MOR. c–e, Time-course reaction profiles for Pt/H-MOR-catalyzed depolymerization of 1 to monomers, showing the selective cleavage of C–C bonds for 2–6 (c), 7–9 (d) and 10–14 (e). a Reaction conditions: 1 (20 mmol l⁻¹), 50 mg catalyst, 40 ml n-pentane, 260 °C, 4 h and 40 bar H₂.

Our results demonstrate an improved total monomer yield of 86.3%, outperforming the previously reported highest yield of 80.7% using a RuRe alloy catalyst. Figure 2b proposes the main reaction pathways during conversion of 1 over Pt/H-MOR, including the major reaction intermediates and products (Supplementary Fig. 4): 2-hydroxybiphenyl (2), 2-cyclohexylphenol (3), 2-phenylcyclohexanol (4), 2-cyclohexylcyclohexanol (5), cyclohexylbenzene (6), dibenzofuran (7), tetrahydrodibenzofuran (8), dodecahydrodibenzofuran (9), bicyclohexyl (10), cyclopentylmethylcyclohexane (11), 3-cyclohexylcyclohexene (12), cyclohexane (13) and methylcyclopentane (14). These pathways are based on the timecourse profiles displayed in Fig. 2c–e, and the rates of the individual reaction steps are provided in Supplementary Table 3. Following an earlier study on the hydrodeoxygenation of guaiacol, we report here pseudo-first-order reaction rate constants to compare the reactivities of the different compounds. Figure 2c shows that 2 is a reaction intermediate obtained by the removal of one of the hydroxyl groups in 1 over Pt. 2 is then partially hydrogenated to 3 and 4 with a reaction rate of 14.6 mmol l⁻¹. 3 and 4 are hydrogenated to 5, and removal of the other hydroxyl group yields 6. Removal of the second hydroxyl group from 5 results in 10 and its isomer 11. Figure 2d demonstrates that 7 is another reaction intermediate obtained from 1 by dehydration over H-MOR with a reaction rate of 15.1 mmol l⁻¹ h⁻¹. Intermediate 7 can be hydrogenated to 8 and 9 with an overall hydrogenation rate of 23.9 mmol l⁻¹ h⁻¹. Intermediates 8 and 9 can then be converted to 6 and 10 + 11. C–C bond cleavage in 10 results in the main monomeric products 13 and 14 with an overall reaction rate of 2.6 mol l⁻¹ h⁻¹ (Fig. 2e). Relevant to cleavage of the alkyl–alkyl moiety in 10 is the observation of compound 12 with a C=C bond that allows C–C bond cleavage via β-scission over H-MOR.

Note that 10 was not converted by Pt catalysts supported on SiO₂, Nb₂O₅, Al₂O₃ and TiO₂ containing Lewis acid and basic sites (Supplementary Table 4). This demonstrates that the Brønsted acid sites in H-MOR are indispensable for alkyl–alkyl cleavage. The cracking of 6 should also be considered as a pathway to the monocyclic products.

The contributions of cracking via intermediates 10 and 6 were then investigated by studying their conversions in separate experiments. The conversion of bicyclohexyl (10) over Pt/H-MOR resulted in 13 and 14 as monocyclic products (Supplementary Fig. 5a), confirming that alkyl–alkyl bonds can be cracked by our approach. Unlike for 1, the conversion of 10 led to heavier products (Supplementary Note 2). Cracking was also achieved with a physical mixture of Pt/SiO₂ and H-MOR (Supplementary Fig. 5b), but not with Pt/SiO₂ or H-MOR (Supplementary Table 4). This confirms the bifunctional nature of the cleavage of 10. Different from the conversion of 1, cyclohexylcyclohexene (12) was not observed during the conversion of 10. However, by lowering the hydrogen pressure to 5 bar, this intermediate was observed (Supplementary Fig. 6). A specific aspect of bifunctional hydrocracking of hydrocarbons is that the distance between the two catalytic functions affects the overall rate. In the present work, this is evident from the substantially higher C–C cleavage rate of 10 for Pt/H-MOR (2.6 mmol l⁻¹ h⁻¹) than for the physical mixture of Pt/SiO₂ and H-MOR (0.8 mmol l⁻¹ h⁻¹), suggesting that slow diffusion of unsaturated intermediates between Pt and acid sites suppresses the overall rate. We then studied C–C cleavage in the unsaturated intermediate cyclohexylbenzene (6) observed during the conversion of 1 over H-MOR without hydrogen (Supplementary Fig. 7a). Products 13, 14 and benzene (15) were formed as the main monocyclic products, confirming that the aryl–alkyl moiety in 6 can be directly cleaved by H-MOR. The observation of small amounts of cyclohexene (16) and 1-methylcyclopentene (17) suggests that dehydrogenation of the cyclohexyl ring in 6 is a possible pathway. The observation of H₂ in the gas phase during this experiment confirms this (Supplementary Fig. 8). Al₂O₃ with mainly Lewis sites did not convert 6 under identical reaction conditions. This further supports the conclusion that strong Brønsted acid sites in H-MOR are the active centers for aryl–alkyl cleavage. Notably, the conversion of 6 on Pt/H-MOR under a H₂ pressure of 40 bar (Supplementary Fig. 7b) led to the formation of similar products. However, products 16 and 17 were not observed, presumably because they were rapidly hydrogenated. The reaction rate of 51.1 mmol l⁻¹ h⁻¹ obtained with Pt/H-MOR was more than five times higher than with H-MOR.

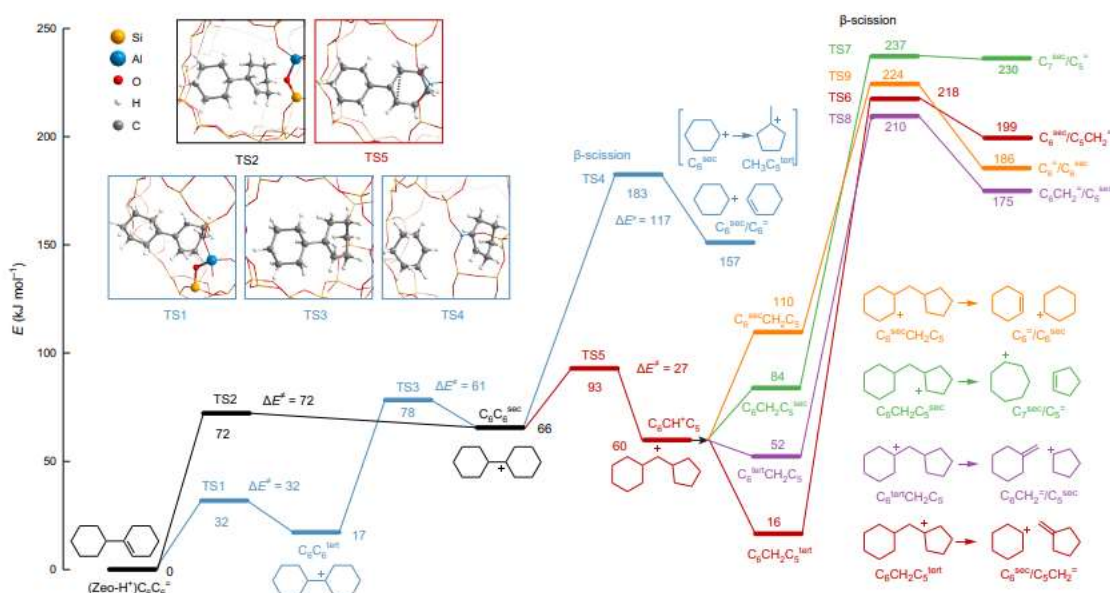


Figure 3 - DFT study of the reaction mechanism of C–C bond cleavage

Potential energy diagram for proposed reaction pathways of C–C bond cleavage in 12 over H-FAU zeolite. Energies are given with respect to the adsorption state of [(Zeo–H⁺)C₆C₆ =]. The most important transition states are shown top left.

This difference is a strong indication that, although direct cracking of 6 on strong acid sites is possible, the bifunctional conversion of 6 via phenylcyclohexene is much faster. From the model compound studies, we can infer that 1 is mainly converted through hydrocracking of 6 with a small contribution of cracking via 10. This is further supported by the nearly similar yields of 13 and 14 during the conversion of 1 and 6, while the conversion of 10 also led to heavier products. To gain a molecular-level understanding of the C–C bond cleavage mechanism over zeolitic Brønsted acid sites, we performed density functional theory (DFT) calculations. To facilitate such calculations for zeolite, we employed an H-FAU zeolite model (Supplementary Fig. 9) instead of H-MOR. Compared with the more complex MOR topology, the faujasite zeolite topology comprises a network of uniform supercages with only one crystallographically distinct T site. Catalytic experiments showed that H-MOR and H-FAU display comparable catalytic behavior (Supplementary Table 5). Various reaction pathways were explored for the cracking of the C–C bond in 12 (1-cyclohexylcyclohexene, $C_6C_6^{\ominus}$) (Fig. 3), which was observed as an intermediate in the cracking of 10. The activation of $C_6C_6^{\ominus}$ over zeolite Brønsted acid sites ($Zeo-H^+$) occurs via protonation of the C–C double bond, which proceeds either via transition state 1 (TS1) to a tertiary carbenium ion (C_6C_6 tert) or via TS2 to a secondary carbenium ion (C_6C_6 sec). As expected, forming a tertiary carbenium ion requires a lower reaction barrier ($\Delta E^{\ddagger} = 32 \text{ kJ mol}^{-1}$) than that of a secondary carbenium ion ($\Delta E^{\ddagger} = 72 \text{ kJ mol}^{-1}$). The conversion of C_6C_6 tert to C_6C_6 sec can be achieved by a 1,2-H shift (TS3, $\Delta E^{\ddagger} = 61 \text{ kJ mol}^{-1}$), which is followed by C–C bond cleavage to form the C_6 products 13 and 14. The cracking of the C_6C_6 sec carbenium occurs via β -scission (TS4, $\Delta E^{\ddagger} = 117 \text{ kJ mol}^{-1}$), which yields a secondary C_6 carbenium along with cyclohexene (C_6 sec/ C_6^{\ominus}). C_6 sec can deprotonate to another cyclohexene molecule or isomerize to a branched 5-ring structure (CH_3C_5 tert). The isomerization of C_6 sec to CH_3C_5 tert occurs in two steps, in which C_6 sec is first rearranged to CH_3C_5 sec and then to CH_3C_5 tert via a 1,2-H shift with respective activation barriers of 52 and 33 kJ mol^{-1} (Supplementary Fig. 10). The deprotonation of C_6 sec and CH_3C_5 tert yields cyclic alkenes, which will be hydrogenated to cyclohexane and methylcyclopentane in the presence of a hydrogenation function such as Pt. As cyclohexane and methylcyclopentane were observed as the main products during the conversion of 10, it is reasonable to conclude that C–C bond cleavage can also occur via intermediates with a cyclohexyl–methylene–cyclopentane skeleton. DFT calculations indicate that forming such intermediates (for example, $C_6CH^+C_5$) is facile via isomerization of C_6C_6 sec with a relatively low barrier (TS5, $\Delta E^{\ddagger} = 27 \text{ kJ mol}^{-1}$). To obtain two cyclic compounds via β -scission, the $C_6CH^+C_5$ intermediate should be converted to a carbenium ion with the positive carbon center either in the 5-ring or the 6-ring ($C_6CH_2C_5$ tert, $C_6CH_2C_5$ sec, C_6 tert CH_2C_5 and C_6 sec CH_2C_5). The formation and interconversion of these carbenium ions can be achieved by intramolecular H shifts with activation barriers in the range of 3–58 kJ mol^{-1} (Supplementary Fig. 11). Depending on the location of the positive carbon center, β -scission of $C_6CH^+C_5$ -derived carbenium ions (TS6–9) leads to

different combinations of cyclic reaction products (Supplementary Fig. 12).

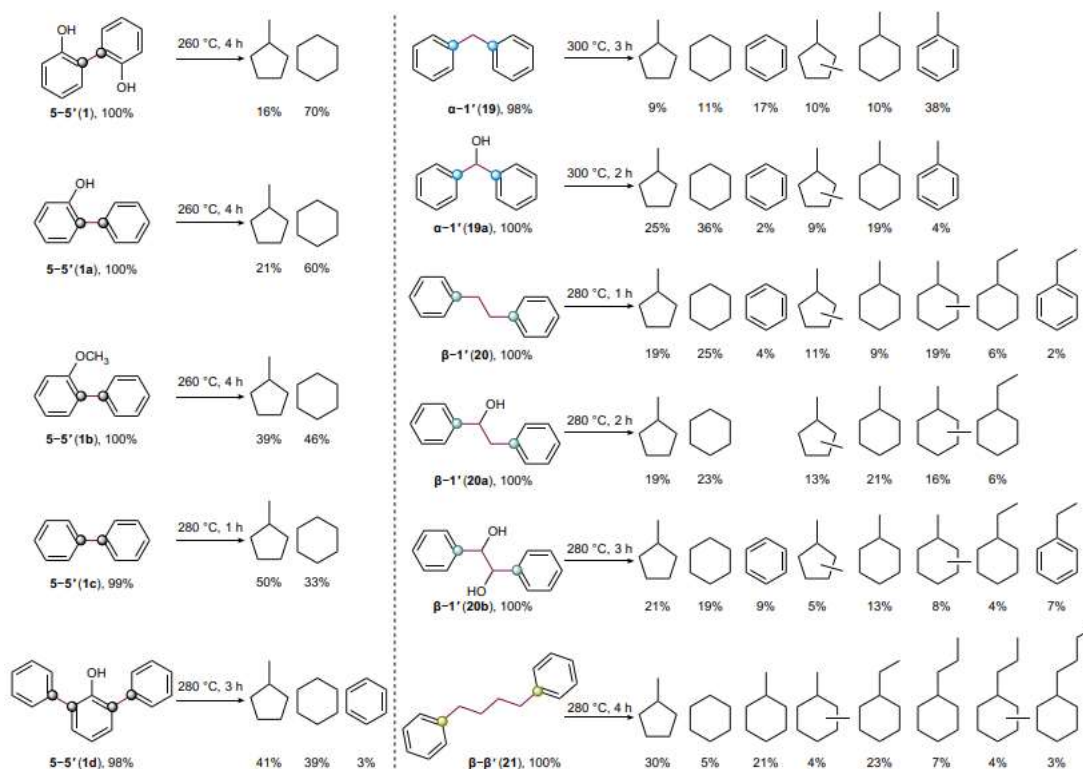


Figure 4 - Substrate scope for reductive C–C cleavage

The numbers below each substrate and product refer to the conversion and yield, respectively. Detailed calculations of these parameters are provided in the Supplementary Information. Reaction conditions: substrate (20 mmol l⁻¹), 50 mg Pt/H-MOR, 40 ml of n-pentane and 40 bar H₂.

A comparison of the energy profiles indicates that these C–C bond cleavage pathways may provide an alternative to β-scission from C₆C₆ sec, although the latter route remains the most favorable (Fig. 3 and Supplementary Table 6). Additional DFT calculations (Supplementary Note 3) demonstrate that a reaction pathway for the C–C cracking of phenylcyclohexene has a low barrier of 86 kJ mol⁻¹, which compares favorably with the barrier of 117 kJ mol⁻¹ for cyclohexylcyclohexene. This explains the preference for C–C cleavage in 6 over 10. Moreover, the direct C–C bond cleavage in phenylcyclohexane is also possible with a barrier of 134 kJ mol⁻¹. These results can explain the experimental finding that, although monomer formation from 6 is possible with H-MOR, the rate with Pt/H-MOR is much higher. Based on this comprehensive understanding of C–C cleavage, we explored different substrates (Fig. 4). Biphenols substituted at the 2-2'-positions were evaluated at a reaction temperature of 260 °C. It is encouraging that different 2,2'-substituents (1a and 1b) also led to monocyclic products in good yields. A substrate without hydroxyls (1c) required a higher reaction temperature (280 °C) to achieve a decent conversion to monocyclic products. Besides biphenol compounds with 5–5' bonds, compounds with β–1' linkages with hydroxyls placed at different positions at the carbon bridge were also evaluated. Conversion of such β–1' linkages (20, 20a and 20b) required a temperature of 280 °C. The lower reactivity of such compounds compared to 1a, 1b and 1c indicates that oxygen-containing substituents on the aromatic ring facilitate hydrogenation and subsequent aryl–alkyl cleavage. In addition to β–1', bicyclic model compounds with methylene linkages (19 and 19a) representing α–1' bonds were converted. Such bonds are typically found in technical lignins due to self-condensation or formaldehyde-induced condensation of lignin fragments during acidic and alkaline fractionation. Compared with 5–5' and β–1' bonds, achieving a high yield of monocyclic products by cleavage of the α–1' bonds in 19 and 19a demanded a higher reaction temperature of 300 °C.

The increase in the temperature required to selectively cleave 5–5', β -1' and α -1' bonds did not correlate with their bond dissociation energies, suggesting that C–C cleavage was also affected by other aspects such as the presence of hydroxyl groups on the aromatic ring in the β -1' linkage. 1,4-Diphenylbutane (21), employed to represent the β - β' linkage, could be converted to monocyclic hydrocarbons with a yield of 98%. It was also found that a bulkier trimer compound (5–5' trimer, 1d) could be decomposed into monocyclic compounds with a high yield at a temperature of 280 °C, further confirming the promise of our approach. With a reliable approach for selectively cleaving C–C bonds in hand, we were motivated to examine the potential of depolymerizing oligomers obtained by aldehyde-assisted fractionation (AAF oligomers; Extended Data Table 1 and Fig. 5). The feedstock was obtained by fractionation of hardwood using isobutyraldehyde as a capping agent to hinder recondensation, followed by catalytic hydrogenolysis of the isolated lignin. The depolymerization of these AAF oligomers over Pt/H-MOR yielded 54.0% monocyclics at 300 °C (Extended Data Table 1 and Supplementary Table 7). For comparison, hydrogenolysis with Pt/C as a catalyst and oxidation with alkaline nitrobenzene oxidation (NBO) gave respective monomer yields of 10.6% (Extended Data Table 1 and Supplementary Table 8) and 9.5% (Extended Data Table 1 and Supplementary Table 9), suggesting that the monomer yield related to C–O bond cleavage was ~10%. Thus, the fivefold increase to 54.0% in monomer yield over Pt/H-MOR results from C–C bond cleavage, in line with the predominance of such linkages in the AAF oligomers (Fig. 5a and Supplementary Table 10). C–C bond cleavage was confirmed by observing partially hydrogenated bicyclic compounds after 1 h and their cleavage to monomers after 4 h (Supplementary Figs. 13 and 14). Whereas five different dimeric compounds containing β - β' , 5–5', α -1', β -5' and β -1' linkages were observed in the lignin oil obtained with Pt/C (Supplementary Fig. 15), these compounds were absent with Pt/H-MOR as the catalyst (Supplementary Fig. 16). The occurrence of C–C cleavage was further supported by a comparison of 1 H/13C 2D heteronuclear single quantum coherence (HSQC) spectra of the AAF oligomers (Fig. 5a) and the lignin oils extracted upon conversion with Pt/C (Fig. 5b) and Pt/H-MOR (Fig. 5c). The AAF oligomers were composed of S (syringyl)-derived phenylpropanol, G (guaiacyl) and H (p-hydroxyphenyl) building blocks with an S/G/H ratio of 64.8/34.8/0.4, which are connected by β -O-4' (A), β -5' (B) and β - β' (C) linkages. After depolymerization, the β -5' (B1) and β - β' (C3) linkages remained intact, with Pt/C (Fig. 5b,d) accounting for 9.8% of the C9 units in the reacted lignin, similar to the content in the parent lignin. In contrast, β -5' and β - β' bonds were completely cleaved with Pt/H-MOR (Fig. 5c,d).

Correspondingly, the H content of the lignin oil obtained with Pt/C slightly increased to 1.2%

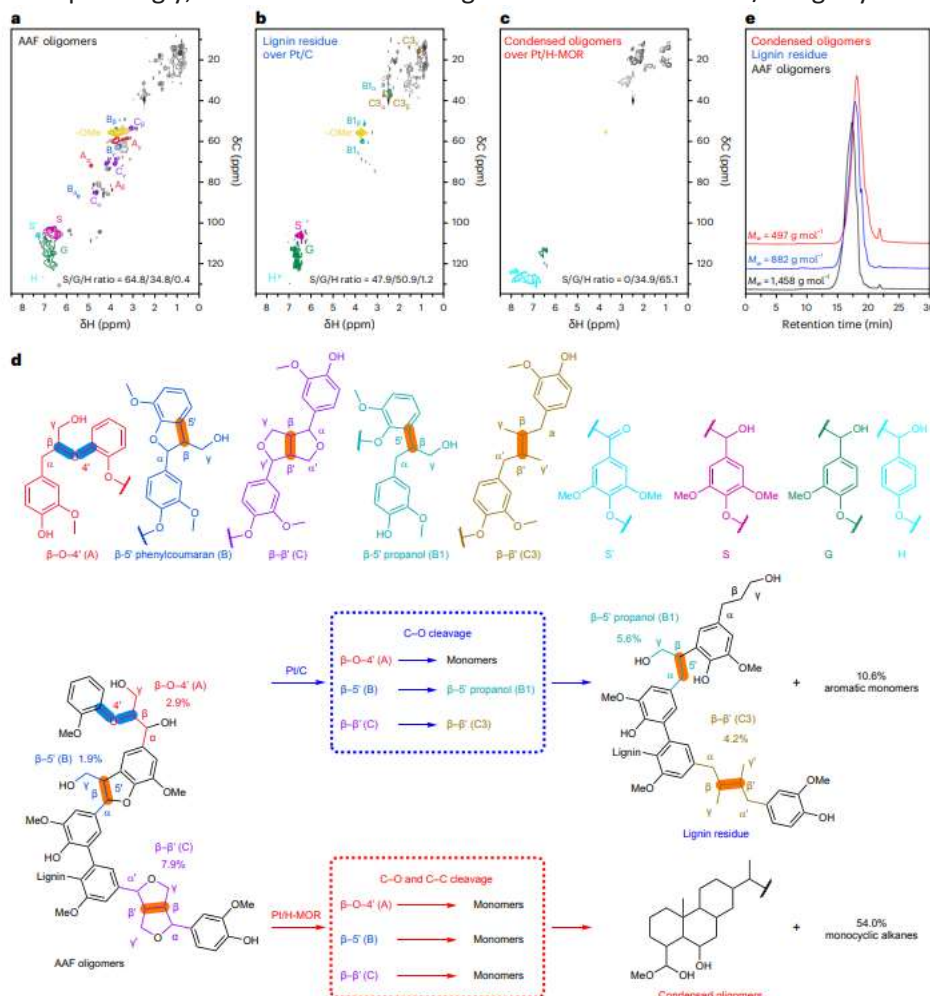


Figure 5 - Reductive cleavage of AAF oligomers

a–c, 2D HSQC NMR spectra of AAF oligomers (a), lignin oil after hydrogenolysis of AAF oligomers over Pt/C (b) and lignin oil after hydrocracking of AAF oligomers over Pt/H-MOR (c). Reaction conditions: AAF oligomers (1.0 g), 500 mg 1 wt% Pt/H-MOR or 100 mg commercial 5 wt% Pt/C, 40 ml of n-pentane, 300 °C, 40 bar H₂ and 24 h. d, Hydrogenolysis of AAF oligomers over Pt/C resulted in a monomer yield of 10.6% via C–O cleavage. A substantially improved monomer yield of 54.0% over Pt/H-MOR was achieved via reductive C–C and C–O cleavage developed using Pt/H-MOR. e, GPC of AAF oligomers (black line), lignin oil obtained after hydrogenolysis of AAF oligomers over Pt/C (blue) and lignin oil obtained after hydrocracking of AAF oligomers over Pt/H-MOR (red).

(S/G/H = 47.9/50.9/1.2), which was accompanied by a decrease in the number of methoxy groups. The increase in the H content to 65.1% (0/34.9/65.1) with Pt/H-MOR can be explained by the high deoxygenation activity of our catalyst. The use of the bifunctional Pt/H-MOR catalyst led to a significant reduction of the molecular weight (M_w) of the condensed oligomers to 497 g mol^{-1} , in comparison with the value of 882 g mol^{-1} for the lignin residue obtained with Pt/C, as determined by gel permeation chromatography (GPC; Fig. 5e). The Pt/H-MOR catalyst could be reused at least four times without any loss of activity in the conversion of AAF oligomers (Supplementary Note 4). The utility of our approach was further assessed in the upgrading of lignin oligomers obtained by the RCF of birchwood. The RCF step yielded a lignin oil containing 42.3% monomers. Further conversion of the lignin oil over Pt/H-MOR increased the total monomer yield to 76.9%, representing a nearly twofold increase over the theoretical maximum monomer yield (Supplementary Note 5).

The broader utility of our approach towards technical lignin was established for a range of lignins fractionated from hardwood and softwood using methods such as acid methanolysis (methanolysis lignin), sulfite pulping (Kraft lignin), alkaline pulping (soda lignin), alkaline pulping with methanolysis (soda-methanolysis lignin), supercritical water extraction (water-extracted lignin) and acid hydrolysis with enzymolysis (enzymatic-hydrolysis lignin) (detailed information is provided in Supplementary Tables 10–13). In all cases, this approach led to a significant improvement of the monomer yield (Extended Data Table 1), that is, by 16.8% for the methanolysis lignin (Supplementary Fig. 17), 6.0% for the Kraft lignin (Supplementary Fig. 18), 12.0% for the soda lignin (Supplementary Fig. 19), 12.4% for the soda-methanolysis lignin (Supplementary Fig. 20), 8.6% for the water-extracted lignin (Supplementary Fig. 21) and 7.9% for the enzymatic-hydrolysis lignin (Supplementary Fig. 22), referenced to values obtained by NBO and Pt/C hydrogenolysis. The HSQC and GPC results (Fig. 5 and Supplementary Figs. 17–22) showed that the β -5' and β - β' linkages in the seven lignins were completely cleaved during their conversion with the Pt/H-MOR catalyst, while most remained intact with Pt/C. This difference illustrates that the type of C–C linkage did not significantly affect the monomer yield achieved by our approach. Among the significant improvements in monomer yield, the extent of C–C cleavage was highest for the AAF oligomers. Comparison of typical properties that can serve as indicators to predict the monomer yield, such as β -O-4' content¹² (Supplementary Fig. 23a), S/G ratio (Supplementary Fig. 23b) and molecular weight (Supplementary Fig. 23c), did not provide a satisfactory explanation for the outstanding results obtained with the AAF oligomers. Instead, we speculate that the H content plays an important role (Supplementary Fig. 23d). Although the water-extracted lignin has a higher H content than the AAF oligomers, it is poorly soluble in various apolar solvents, which can explain the poor C–C cleavage performance in our approach. The substrate scope study showed that cleaving the C–C bond in the compound representing H units (1 in Fig. 4) is much easier than others. This aspect can be further utilized in future studies by employing a larger population of natural variants to perform multivariate studies. We then designed a process involving our C–C bond cleavage approach (Fig. 6a, Supplementary Fig. 24 and Supplementary Table 14) to perform a techno-economic analysis (TEA) and a life-cycle assessment (LCA) for a biorefinery based on AAF oligomers. The process involves the complete hydrodeoxygenation (HDO) of the intermediates obtained by the C–C bond cleavage strategy. The product consists of alkylated cyclohexanes and monoaromatics with a gasoline-range C₆–C₈ fraction (74.9%) and a fraction of C₉–C₁₀ compounds (25.1%), which can be blended with (renewable) jet fuel (Supplementary Table 15). Renewable jet fuel can be derived from various sources, such as synthetic paraffinic kerosene (SPK) obtained by Fischer–Tropsch synthesis, biomass-derived synthetic paraffinic kerosene (Bio-SPK) and hydroprocessed esters and fatty acids (HEFA) from animal fats and plant oils, which mainly consist of n- and iso-alkanes. According to ASTM D7566-14a, jet fuel should contain at least 8 vol% of aromatics and up to 15 vol% of cycloalkanes, which can be obtained from the proposed catalytic process by liquid–solid separation (separator 1) and liquid fractionation (separators 3 and 5). The water formed during lignin HDO ends up in the wastewater stream from separator 4. The gaseous mixture comprising C₁–C₄ gases, n-pentane and H₂ is fed to the condenser (separator 2), in which n-pentane, together with the collected n-pentane and biofuel from separator 4, is recycled back to the reactor. The remaining gas mixture of C₁–C₄ hydrocarbons and H₂ is processed in the pressure swing adsorption (PSA) section, separating the C₁–C₄ components from H₂, the latter being recycled to the reactor. The C₁–C₄ gas and the lignin residue from separator 1 are combusted for heat recovery. The mass flows in Fig. 6b (also Supplementary Tables 16 and 17) show that the conversion of 2,000 tons of AAF oligomers yields 270.1 tons of jet fuel and 809.0 tons of gasoline, corresponding to 54 wt% of the lignin intake. The HDO process consumes 24% of the H₂, while 2% of the H₂ is lost in the liquid–gas separation and PSA processes. Analysis of the carbon-based flows (Supplementary Fig. 25) reveals that 49.9% of lignin is converted to jet fuel-compatible mixtures, gasoline, lignin residue and gas with carbon yields of 21.1%, 63.3%, 12.9% and 2.8%, respectively. The remaining lignin (50.1%) was burned for energy. The energy flows (Supplementary Fig. 26 and Supplementary Table 18) demonstrate that operating the biorefinery necessitates the additional combustion of lignin to fulfill the remaining 39.4% of the energy requirement. The TEA of the proposed biorefinery (Fig. 6c) was calculated for a daily treatment of 2,000 tons of lignin. The combustor (32.7%) and high-pressure reactor (25.3%) were the most expensive pieces of equipment (Supplementary Fig. 27). Concerning operational expenditure, the feedstock was the most significant contributor to the manufacturing cost (Supplementary Fig. 28 and Supplementary Tables 19 and 20).

Eight different scenarios (Supplementary Table 21) were compared, considering the mode of H₂ consumption, H₂ recycle, solvent loss and feedstock/product combustion on the operating cost. The minimum fuel selling price (MFSP) was determined using a 10% discount rate without considering taxation. The selling price of the product was adjusted to achieve a net present value (NPV) of zero. Based on the design and economic basis (Supplementary Table 22), scenario I reached the lowest MFSP of US\$1.51 per gasoline gallon equivalent (GGE). This was mainly due to the higher yield of target products, such as gasoline, and the reduced solvent consumption through lignin combustion. Given the current pricing of jet fuel and gasoline, the optimized scenario I offers a rough internal rate of return of 23.0% and a payout time of 6.6 years for a plant with a lifetime of 20 years (Supplementary Table 23). We also carried out an LCA of this process (Fig. 6d, Supplementary Fig. 29 and Supplementary Tables 24–27).

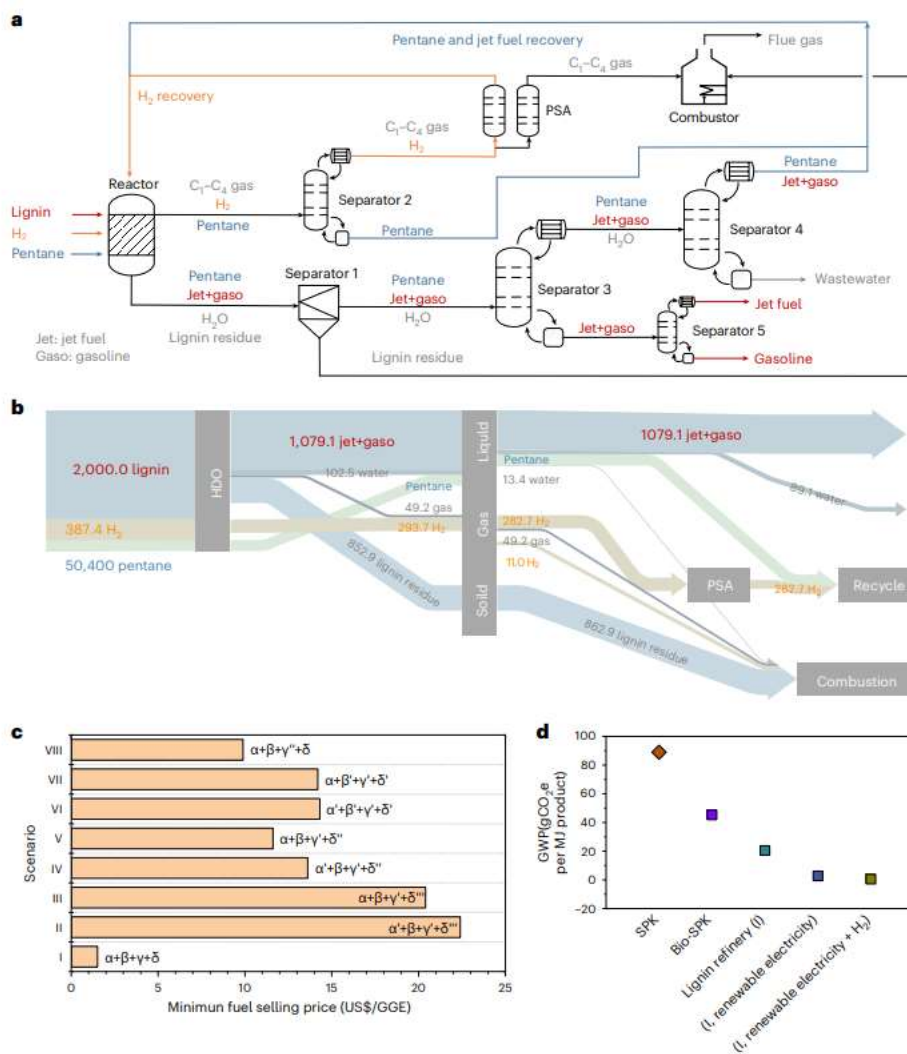


Figure 6 - Process layout and details of the proposed AAF oligomers refinery.

a, Proposed block flow diagram to produce jet fuel and gasoline components from the reductive cleavage of C–C bonds in lignin. **b**, Mass flows (t d⁻¹) of the lignin biorefinery. **c**, Minimum jet fuel selling price (MFSP) for various scenarios based on a West Texas Intermediate (WTI) price of US\$96.5 per barrel and a gasoline price of US\$1,161.1 per ton. H₂ consumption is based on the oxygen content in the model compound (β -O-4', α) and lignin (elemental analysis, α'); H₂ recycle: Yes (β) and No (β'); combustion of lignin (γ), pentane (γ'), and gasoline and lignin (γ''); solvent loss at 0.2% (δ), 1% (δ'), 3% (δ'') and 5% (δ'''). **d**, Global warming potential (GWP) (gCO₂e per MJ product) of biofuel in different scenarios.

Optimized scenario I was compared to standard scenarios, including SPK43 and Bio-SPK44. As expected, scenario I showed the lowest greenhouse-gas emissions at 20.4 gCO₂e MJ⁻¹ jet fuel and gasoline, giving respective decreases of 55.0% and 77.1% compared to Bio-SPK and SPK. The greenhouse-gas emissions would

decrease to 0.47 gCO₂e MJ⁻¹ jet fuel and gasoline using renewable electricity and H₂, unveiling the possibility for a CO₂-neutral lignin biorefinery aimed at fuel production. Current biorefining efforts remain strongly hampered by the low value of lignin waste, even when part of the lignin can be valorized into valuable building blocks in the lignin-first approach. The present study demonstrates a technology to convert recalcitrant lignin sources rich in C–C bonds into valuable products for sustainable aviation purposes, contributing to reducing the carbon footprint of this hard-to-abate sector in terms of greenhouse-gas emissions. The developed catalytic approach selectively disrupts various C–C linkages without pre-functionalization under relatively mild conditions. It is based on the synergistic action between a Pt (de)hydrogenation function and Brønsted acid sites confined in the micropores of zeolite. We have demonstrated that this hydrocracking strategy is effective for upgrading oligomers obtained by aldehyde-assisted fractionation or RCF from lignocellulosic biomass, as well as various technical lignins, underpinning the broad utility of our approach. As such, this technology can be easily integrated into different biorefining schemes, bringing the valorization of some 70 million tons of lignin waste annually produced closer to reality.

3 Conclusions

Carbon–carbon bonds, ubiquitous in lignin, limit monomer yields from current depolymerization strategies, which mainly target C–O bonds. Selective cleavage of the inherently inert σ -type C–C bonds without pre-functionalization remains challenging. Here we report the breaking of C–C bonds in lignin obtained upon initial disruption of labile C–O bonds, achieving monocyclic hydrocarbon yields up to an order of magnitude higher than previously reported. The use of a Pt (de)hydrogenation function leads to olefinic groups close to recalcitrant C–C bonds, which can undergo β -scission over zeolitic Brønsted acid sites. After confirming that this approach can selectively cleave common C–C linkages ($5-5'$, $\beta-1'$, $\beta-5'$ and $\beta-\beta'$) in lignin skeletons, we demonstrate its utility in the valorization of various representative lignins. A techno-economic analysis shows the promise of our method for producing gasoline- and jet-range cycloalkanes and aromatics, while a life-cycle assessment confirms its potential for CO₂-neutral fuel production.

Acknowledgement

The author(s) would like to thank the partners in the project for their valuable comments on previous drafts and for performing the review.

Project partners:

#	Partner short name	Partner Full Name
1	TUE	Technische Universiteit Eindhoven
2	VERT	Vertoro BV
3	T4F	Tec4Fuels
4	BLOOM	Bloom Biorenewables Ltd
5	UNR	Uniresearch B.V.
6	WinGD	Winterthur Gas & Diesel AG
7		(Formerly SeaNRG, is now GOODFUELS #12)
8	TKMS	Thyssenkrupp Marine Systems GMBH
9	OWI	OWI – Science for Fuels gGmbH
10	CSIC	Agencia Estatal Consejo Superior De Investigaciones Cientificas
11	VARO	Varo Energy Netherlands BV
12	GOOD	GoodFuels B.V.



This project has received funding from the European Union's Horizon 2020 research and innovation programme under grant agreement No 883753